Single dispersive gradient-index profile for the aging human lens

José Antonio Díaz,[1,*] Carles Pizarro,[2] and Josep Arasa[2]

[1]*Departamento de Óptica, Edificio Mecenas, Universidad de Granada, 18071-Granada, Spain*
[2]*Center for Sensors, Instrumentation and Systems Development, Universitat Politècnica de Catalunya, Rambla Sant Nebridi 10, Terrassa 08222, Spain*
[*]*Corresponding author: jadiaz@ugr.es*

Received May 8, 2007; revised October 23, 2007; accepted November 4, 2007;
posted November 15, 2007 (Doc. ID 82797); published December 21, 2007

We provide a single gradient-index (GRIN) profile for the crystalline lens in an updated age-dependent emmetropic-eye model. The parameters defining the GRIN profile include their variation with age and the dispersion of the refractive index in order to account for the increase in the positive-wave spherical aberration, for the constant chromatic difference in the refraction of the human eye, as well as for the decrease in the retinal-image quality with aging. In accounting for these ocular properties, the results show that first, the value of the dispersion parameters are invariant with age. Second, those parameters defining the distribution of the lens index cause the lens-center-index value to decrease slightly, and its position along the lens axis changes with age. Furthermore, these findings are in agreement with the lens paradox. © 2007 Optical Society of America

OCIS codes: 330.5370, 110.2760, 170.4460.

1. INTRODUCTION

The structure of the crystalline lens in the human eye is known to be layered [1,2]. Based on this, Gullstrand [3] was the first researcher who proposed eye models in which the lens had an inhomogeneous index distribution: One of them had a two-shell-index lens, and a second one had a continuous index distribution. In the late 20th century, several investigators proposed a lens that had a GRIN (gradient-index) distribution. These profiles were used in more realistic eye models in an attempt to explain the mean retinal-image quality of the population in relaxed emmetropic as well as in myopic eyes, and for the former ones, even in various states of accommodation [4–9].

Many studies have attempted to measure the refractive index distribution of crystalline lenses using different experimental techniques applied to *in vitro* [10–21] as well as to *in vivo* [22–25] animal and human lenses. However, the results suffer from low resolution, or they have to assume constraints for the index distribution to conform to a particular model. The lens is the optical element in the eye that undergoes noticeable changes with age and accommodation. There is a good agreement in the physiological optics community that a complete lens based on reliable measurements of its index distribution is needed, given that schematic eye models are used in modeling several popular surgical techniques, such as refractive surgery [26–28], intraocular implants [29,30], as well as vision applications [31–33]. Furthermore, since eye aberrations change with age [34–36] and accommodation [37–39], these techniques can be better predicted and simulated with a schematic eye having a lens model that accounts for these changes.

The current profile proposed for the human lens has an asymmetric elliptical shape for isoindicial surfaces, but some studies question whether these elliptical surfaces should be concentric [10]. Due to the asymmetry of the index distribution along the axis of this kind of profile, the GRIN lens profile can be modeled in two parts (Fig. 1, top). That is, the lens is assumed to be composed of two plano–aspheric components, each having a specific GRIN distribution and being in contact with the plane surfaces [7,9]. In fact, this does not lead to a real two-element crystalline lens; instead, the plane surface is a dummy surface that eases GRIN profile modeling. Of course, the index values and their gradients must be continuous on this contact-plane surface.

In addition to the model proposed by Gullstrand, a single profile to describe the index distribution for the whole crystalline lens (Fig. 1, bottom) has been reported to account for various states of accommodation [4,8,40,41]. The most recent [41] is based on the model proposed by Liou and Brennan [7], but the lens is replaced by a new one with a single GRIN distribution. However, the above-mentioned studies did not compare data with the experimental results in the literature, such as the modulation transfer function (MTF) or the eye spherical aberration, i.e., wave spherical aberration (SA).

With respect to the dependence on aging, several studies have shown that vision quality declines with age [34–36,42–44]. Some efforts have been made to model the geometry of the cornea and the human lens with age [5,45–50]. It is well known that the lens-surface radii of curvature decreases with age. If the lens refractive index remains constant with age, the lens power should increase. This effect implies that an emmetropic subject turns myopic over the years; however this is not true. This is known as the lens paradox, and many efforts from the standpoint of modeling the lens GRIN profile [51,52], as well as from experimental measurement of *in vitro* hu-

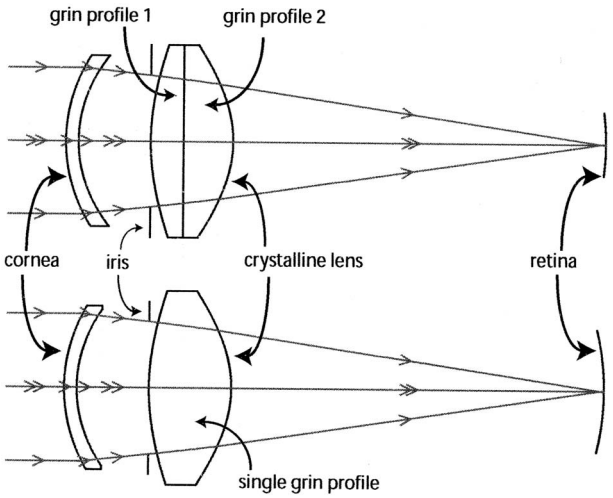

Fig. 1. Modeling the crystalline lens in current eye models with two GRIN profiles (top) and with a single profile.

man lenses, have been made to explain why an emmetropic eye maintains its power with age [19,53,54]. It has been deduced from these studies that an alteration of the GRIN profile as well as a variation in the internal refractive index value could provide the explanation. However, a recent study [21] points to the fact that the lens-center index does not change with age and that the size of the central index plateau increases in size also with age, in agreement with a previously published prediction [50]. In addition, it is known that the lens loses some negative SA with age and thus the ability to compensate for the positive SA of the cornea, and, therefore, the eye augments its positive SA as age progresses [44].

A complete model for the human-lens refractive index also should include its variation with wavelength. Liou and Brennan [7] proposed for their eye model a waterlike dispersion not only for the ocular media and the cornea but also for the GRIN lens profile. They justified this selection by observing that the ocular media, including the lens, are composed mainly of water. Nevertheless, it should be considered that their dispersion equation for the lens has, erroneously, a parabolic dependence on wavelength, and it considerably reduces the index value from what it should be [55]. The dispersion of the ocular media is responsible for the eye's longitudinal and transverse chromatic aberrations [56,57], which are considered invariant with age [58,59]. Recently, Atchison and Smith [55] have reported a Cauchylike four-term expression for characterizing the dispersion properties of each ocular medium, including the lens. These authors successfully explain the theoretical and experimental data for ocular media dispersion. Moreover, with these expressions, it is easy to extend the study of visual functions to the near IR.

In this paper, a single GRIN profile is proposed for the human lens. The parameters describing this profile have been reported with age dependence, and the refractive index variation with wavelength has also been included, taking into account the recent data for the lens edge and center [9,21]. This GRIN lens profile has been used in a updated schematic eye model for an emmetropic subject, in which the ocular geometrical parameters also change with age. Furthermore, decentrations and/or tilts of the ocular elements [9,60,61], as well as an ellipsoidal retina [62], have been considered. We have constrained the parameters describing the GRIN profile to account for maintaining eye power as age advances, for the age-independent eye longitudinal chromatic aberration, and for the experimental monochromatic foveal MTF. The later implies that the results for the MTF have been evaluated in the fovea at all ages, and thus the visual axis [7,63] has been introduced in the schematic eye. This aging schematic eye could serve as a starting point in the study, simulation, and prediction of several vision defects and their correction, as well as of the accommodation influence on visual performance.

2. METHODS

Modern optical-design software (ZEMAX-EE, Software Development, Inc.) was used to implement the GRIN profile for modeling the lens of a schematic eye. Regarding this schematic eye model, we have used the up-to-date ocular data concerning curvatures of surfaces, asphericities, thicknesses, and dispersions of ocular media. In addition, since we have modeled the GRIN profile with age, those geometrical parameters for the cornea and the lens have been varied with age according to published data [45–49]. The age-dependent schematic eye model described below has been chosen to be as accurate as possible with the anatomic relative positions of their surfaces. That is, the eye was not considered to be a centered system but a decentered optical system and with the fovea set at 5 deg from the optical axis (angle alpha) [7,63].

A. Cornea

A rotationally symmetric conicoid was adopted for the shape of the corneal surfaces [7,64–66]. Corneal data dependence with age was taken from the recent work of Dubbleman *et al.* [48]. Although they reported variations in the asphericities along the horizontal as well as the vertical corneal axes that lead to spherocylindrical errors, we have discarded this dependence.

Thus, the anterior, R_{c1}, and the posterior, R_{c2}, radii of curvature were taken as 7.79 mm and 6.53 mm, respectively, which were on average independent of age [48]. Regarding the asphericities of the corneal surfaces, both changed with age according to the following:

$$Q_{c1} = -0.24 + 0.003 * age, \qquad Q_{c2} = -0.006 * age. \quad (1)$$

The asphericity, Q, of the surface is defined as $-K$, K being its conic constant [63], and it is related to the conic constant defined by Dubbleman *et al.* [48], k, through the relationship $k = Q + 1$. The refractive index was taken at 555 nm with a value of 1.3759 [7,55,65,66].

B. Anterior Chamber and the Iris

The variation of the anterior chamber depth with age, bearing in mind the adopted corneal thickness of 0.579 mm [45], was given [45] by

$$ACD = 3.87 - 0.01 * age, \tag{2}$$

having a refractive index for the aqueous of 1.3359 at 555 nm [7,55].

The iris, the aperture stop of the eye, was set at the vertex of the anterior lens surface. An average decentration was set at 0.3 mm in the nasal direction. This value averages the data gathered by Liou and Brennan with those of Yang *et al.* [67], in which values as small as 0.2 mm and as large as 0.5 mm were found, and thus an average of 0.3 mm could be adopted for a normal subject in photopic conditions. This decentration value was independent of age, and no vertical decentration was set.

C. Lens

We also adopted a rotationally symmetric conicoid for the shape of lens surfaces [7,9,65,66], and we followed the data reported by Dubbleman *et al.* [46,49]. Their results agree quite well with the mean data in previous works, and their Scheimpflug imaging technique is as reliable as the Purkinge imaging technique [68]. Thus, the radii of curvature of the anterior, R_{l1}, and the posterior, R_{l2}, lens surfaces, and their respective asphericities, Q_{l1} and Q_{l2}, were given as a function of age by

$$R_{l1} = 12.7 - 0.058 * age; \qquad Q_{l1} = -5, \tag{3}$$

$$R_{l2} = -5.9 + 0.0015 * age; \qquad Q_{l2} = -4. \tag{4}$$

The refractive index was modeled bearing in mind that the lens can be regarded as one element having a single continuous GRIN distribution. For this, the GRIN lens profile for the whole lens was given by

$$n(\lambda,x,y,z) = n_0(\lambda) + n_1(\cos(n_2 z) - 1) + n_3 \sin(n_4 z) + n_5(x^2 + y^2), \tag{5}$$

where z is the lens axis, the terms containing the function cos and x^2+y^2 model the elliptical shape of the isoindicial surfaces, and that containing the function sin accounts for its asymmetry along the lens axis. The sine and cosine functions were chosen because they simplify the use of complex polynomials describing the variation of the GRIN profile along the lens axis [41]. As can be seen, the index distribution follows the widely accepted rotationally symmetric model through the dependence on the term x^2+y^2, since this is the square of the distance of any off-axis point to the lens axis (z axis).

The term $n_o(\lambda)$ accounts for the variation of the lens index with wavelength, while the remaining terms account for its spatial distribution. This is a reasonable assumption; although there would be reasons to assume that the constants n_1 to n_5 change with wavelength, it is the simplest one. Thus, n_o was modeled as a function of the wavelength following a Sellmeierlike equation with six constants:

$$n_o^2(\lambda) - 1 = \frac{K_1\lambda^2}{L_1 - \lambda^2} + \frac{K_2\lambda^2}{L_2 - \lambda^2} + \frac{K_3\lambda^2}{L_3 - \lambda^2}, \tag{6}$$

where λ is in nanometers.

This six-constant equation is the common one used for obtaining the dispersion of dielectric materials. It has wide theoretical support, it is easy to implement in modern optical software, and it allows the refractive index to be extended to the near IR [69]. In fact, the Cauchy equation for the dispersion of dielectric media is an approximation of that of Sellmeier when $L_i \gg \lambda$. The value of n at 555 nm was assumed to be a value of 1.371 for the lens edge, regardless of age [21], and a value of 1.418 for the lens center [21], but this is variable in the modeling.

The lens thickness changes with age, and we have taken the data from Dubbleman *et al.* [45,49]; thus

$$d_L = 2.93 + 0.0236 * age. \tag{7}$$

Regarding the tilt and decentration of the lens, we followed the work of Atchison [9], assigning an age-independent tilt of 4 deg to the temporal object space, with no decentration. The lens is tilted with respect to its center. This tilt value agrees with a more recent study from Chang *et al.* [60]. This study also reports a decentration of the lens surfaces with respect to the corneal axis. However, the mean values cover decentrations in different directions, and no conclusive data could be obtained from individual subjects. By using an instrument designed specifically for measuring misalignments of optical surfaces, Tabernero *et al.* [61] also found similar values for the lens tilt and small values for the decentration of the lens for two normal eyes. Consequently, no decentrations are adopted for the lens in this work.

D. Eye Length and the Vitreous Chamber

We have used a paraxial image position to determine the axial eye length. This is a widely used condition when working with schematic eye models, and it gives a value for the axial eye length of 23.59 mm for a 25-year-old emmetropic subject at 555 nm. This length is consistent with previous experimental data [9], and it was assumed to be constant over age. The vitreous chamber then changes with age according to the expression

$$VC = 16.79 - 0.0136 * age. \tag{8}$$

The refractive index value of the vitreous humor at that wavelength was 1.3359 [7,55,65,66].

E. Retina and the Position of the Fovea

The retina was set at the paraxial image plane. In addition, its shape was adopted following the work of Atchison *et al.* [9,21] independently of age. Thus, a tilted and decentered ellipsoid was considered the radii of −12.91 mm in the horizontal section and −12.72 mm in the vertical section. The corresponding asphericities were 0.27 and 0.25.

Because the visual axis goes to the fovea and the gaze of a subject points to it in the image space, we have introduced the fact that the fovea was not on the optical axis of the eye but at 5 deg to the horizontal temporal direction [7,63]. This angle, called the angle alpha, was set in the schematic eye model as the angle made by the chief ray at the exit from the posterior lens surface with the corneal axis. This position of the fovea was assigned as the reference position for all calculations concerning retinal-image quality and ocular aberrations.

F. Dispersion of Ocular Media

As indicated, the dispersion of the cornea, the aqueous, and the vitreous humor were taken from the work of Atchison and Smith [55].

Taking into account all these data, Fig. 2 is the right eye modeled (top view) of an emmetropic subject, and Table 1 lists the parameters defining the schematic eye model as a function of age at 555 nm wavelength.

G. Fitting Lens Parameters with Age

To determine the GRIN lens distribution with aging, we have considered that simulated emmetropic subjects from 20 to 65 years old, in steps of 5 years, should resemble the monochromatic foveal MTF, the eye SA, and the longitudinal eye chromatic aberration of actual emmetropic subjects.

Thus, on the one hand, the average value for the eye SA at 555 nm was taken into account at 25 years [7,9]. On the other hand, the experimental monochromatic MTF data taken as reference were those from previous works [34,42]. In a subsequent paper from McLellan *et al.* [35], the MTF was determined for different subjects ranging in age from 23 to 65 years. Comparing their results with those of Guirao *et al.* [34], we found that the MTF declines with aging similarly, but has higher values, especially at spatial frequencies greater than 30 cycles per degree (cpd). The differences where explained due to the dissimilar experimental methods used in the two works regarding ocular scattering. Thus, we took the functions that fit the MTF data from Guirao *et al.* corresponding to the representative three groups of subjects using a monochromatic wavelength value of 543 nm and a 6 mm pupil diameter without apodization—that is, we did not take the Stiles–Crawford effect into account [70–73]. The functions were sampled to have a total of ten MTF values, for fitting purposes, and a higher weight was assigned for spatial frequencies less than 30 cpd. Because these values are radial average MTF values [34], in our case they were set as the mean value from the vertical and horizontal MTFs calculated by the software.

The dispersion of the ocular media is responsible for the longitudinal chromatic aberration of the human eye [56]. This implies an eye-power difference with the wavelength evaluated as a chromatic difference on refraction [57] (CDRx, in diopters, D), with respect to a reference wavelength, which was 555 nm in the present study. This CDRx was assumed with no dependence on age, as reported in previous studies [58,59]. Thus, in a preliminary approach to obtain the GRIN lens profile parameters, if we determine the dispersion parameters for a given age, these parameters can be maintained as constant over the age range considered if the power of the eye also remains constant.

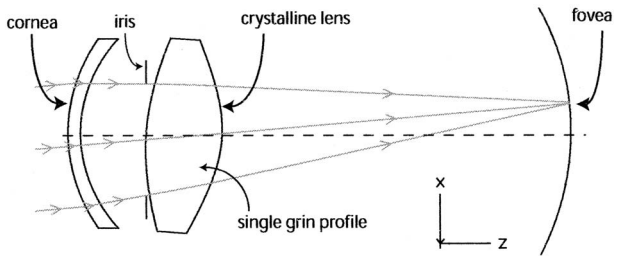

Fig. 2. Example of the schematic eye model used for an emmetropic subject. This view is from the top of the right eye. The right eye was used in all calculations.

Therefore, in an initial approach to modeling the GRIN lens profile, we calculated the parameters that, for a 25-year-old subject, define the profile constrained to resemble the CDRx of the human eye [57], the experimental foveal MTF from Guirao *et al.* [34], and the eye SA at that age. We used a flat spectral illumination having a spectral range from 400 to 700 nm at 25 nm steps, weighted by the luminous efficiency function of the eye [74]. Due to the inaccuracy in the experimental asphericity values of the anterior and posterior lens surfaces, these parameters were also considered as variables in the fitting procedure, given the target value for the average SA. Because the eye modeled was a decentered system, the value for the SA was calculated through the Zernike coefficient Z_4^0 following the double-indexing scheme [75].

Once this first fitting process was completed, we fixed the dispersion terms to be constant over the age range considered as well as over the asphericities of the lens surfaces. Then the variation of the GRIN distribution parameters with aging were determined by a subsequent optimization process that gives the optimum values to resemble the foveal MTF values at all ages considered.

In optical design, there are two main strategies in an optimization procedure: the local-minimum search and the global minimum search [76–78] of a merit function. The latter is time-consuming, and it is suitable for finding a set of starting optical-system solutions for further fine-tuning to the desired results via the finding of a local minimum. In our case, the system to optimize is not far from the desired result. Thus, it is better to perform a local-minimum search by using the least-squares algorithms widely implemented in optical software.

The value of the merit function used is calculated by the root sum square of the weighted optical value differences [76]:

$$\psi = \left[\sum \omega_j^2 (\alpha_j - \alpha_{jt})^2\right]^{1/2}, \tag{9}$$

where ω_j is the weight applied to the jth difference between the actual optical value α_j and the target optical value α_{jt}. In our case, those optical values were the weighted foveal MTF at adopted spatial frequencies and ages, the age-independent CDRx, and the SA at 25 years and 555 nm. We use the DLS (damped least-squares) algorithm for the optimization procedure with the optical software [78].

Some additional constraints were imposed on the optimization process. These constraints force the process to the best solution found to satisfy the established requirements. These were as follows:

1. The eye power was constant over age and was set to 61.27 D at 555 nm. This value corresponds to the eye power of our 25-year-old emmetropic subject.
2. The refractive index of the lens edge was set at 1.371, as several studies have reported [9,21], and it is independent of age.

Table 1. Schematic Eye Parameters as a Function of Age (A)[a]

Surface	Medium	n (555 nm)	R (mm)	Asphericity	Thickness (mm)
1	Cornea	1.376	7.79	$-0.24+0.003^{*}A$	0.579
2	Aqueous	1.336	6.53	$-0.006^{*}A$	$3.291-0.01^{*}A$
3 (iris)[b]	Aqueous	1.336	∞	—	0
4[c]	Lens	$1.371+n_1(\cos(n_2 z)-1)+n_3\sin(n_4 z)+n_5(x^2+y^2)$	$12.7-0.058^{*}A$	−4.56	$2.93+0.0236^{*}A$
5	Vitreous	1.336	$-5.9+0.0015^{*}A$	−1.13	$16.79-0.0136^{*}A$
6 (retina)[d]	—	—	$R_x=-12.91$ $R_y=-12.72$	$Q_x=0.27$ $Q_y=0.25$	—

[a]The index coefficients have a dependence on age, tabulated in Table 2.

[b]The iris is decentered −0.3 mm along the x axis; that is, it is decentered 0.3 mm nasally (see [67]).

[c]The lens is tilted −4 deg about the y axis containing its center; that is, the lens axis is 4 deg to the temporal space object (see [9]).

[d]The retina is an ellipsoid tilted −11.5 deg about the y axis and −3.6 deg about the x axis (see [62]).

3. RESULTS

Table 2 presents the coefficients corresponding to the dispersion term describing the variation of the refractive index with wavelength and the dependence with age of the parameters characterizing the index distribution. As can be seen in Table 2, since these parameters correlated well with age, a linear dependence could be found for them. In Fig. 3, they are plotted as a function of age at 555 nm; also plotted is the linear fit for each parameter. Dashed lines indicate the confidence interval at the 95% level. All these parameters decrease in absolute value with age.

It is informative to analyze the impact of these parameters on the distribution index variation with age. Figure 4 depicts the index contours at 1.371, 1.38, 1.39, 1.40, 1.41, and 1.42 values in an equatorial section (the YZ plane), the index profile along the lens axis (Z axis), and the lens-center-index profile along the equatorial lens radius. We assumed an equatorial lens radius of 4.5 for adult eyes [9]. From this figure, we can see that, in order to explain the retinal-image quality decline with age at a constant eye power, the index of the lens center decreases from 1.417 to 1.407 from 20 to 65 years, respectively. This similar variation in the lens-center-index value has also been reported in experimental works using MRI images of lens donors [19,54]. Moreover, the position within the lens where the index has a high value also varies slightly with age, from 1.326 mm to 1.951 mm at the same age range, which gives a change in the percentage with respect to the total lens thickness from 39% to 43.7%. In the middle column of Fig. 4, the dotted line indicates that position, and we can deduce that this position moves to the geometric center of the lens. It seems therefore that our model predicts that the index distribution of the lens gets more symmetric as age increases.

With respect to the dispersion properties of the lens index, Fig. 5 presents comparisons between the dispersion of the lens-edge index and the lens-center index found in this study by using the dispersion constants in Table 2 and Eq. (6), as well as the data reported by Atchison and Smith [55], rescaled by Atchison [9] to get a refractive index of 1.371 at the edge and 1.418 at the center. Our findings are very close to their data, so that the larger differences occur at the shorter wavelengths, with values of less than 0.002 for those differences.

However, as commented on in Section 2, the dispersion term n_o was kept constant once it was calculated at 25 years, since the CDRx does not significantly vary with age [58,59]. This is reflected in Fig. 6, where the CDRx corresponding to an emmetropic eye at 25 and 65 years is compared with that of the chromatic eye [57]. The agreement is quite good, and the CDRx difference increases at shorter wavelengths. However, given that difference is within the experimental error, our premise about the constant CDRx over age is well predicted by our model.

Table 2. Value of the GRIN Profile Parameters as a Function of Age (A)[a]

Coefficient	Value	p-value	R^2
K_1	−30.121153		
$L_1(\mathrm{nm}^2)$	-19.383097×10^6		
K_2	−0.809941		
$L_2(\mathrm{nm}^2)$	0.017803×10^6		
K_3	−156.88487		
$L_3(\mathrm{nm}^2)$	107.42008×10^6		
n_1	$0.0394(\pm0.0018)-0.000355(\pm0.00004)^{*}A$	$<1\times10^{-4}$	0.907
$n_2(\mathrm{mm}^{-1})$	$1.238(\pm0.031)-0.00561(\pm0.0007)^{*}A$	$<1\times10^{-4}$	0.89
n_3	$0.1092(\pm0.0018)-0.00077(\pm0.000039)^{*}A$	$<1\times10^{-8}$	0.979
$n_4(\mathrm{mm}^{-1})$	$0.79(\pm0.014)-0.00312(\pm0.00032)^{*}A$	$<1\times10^{-4}$	0.921
$n_5(\mathrm{mm}^{-2})$	$-0.00235(\pm0.00002)+1.32\times10^{-5}(\pm5\times10^{-7})^{*}A$	$<1\times10^{-8}$	0.991

[a]The dispersion parameters were independent of age to account for the eye's longitudinal chromatic aberration.

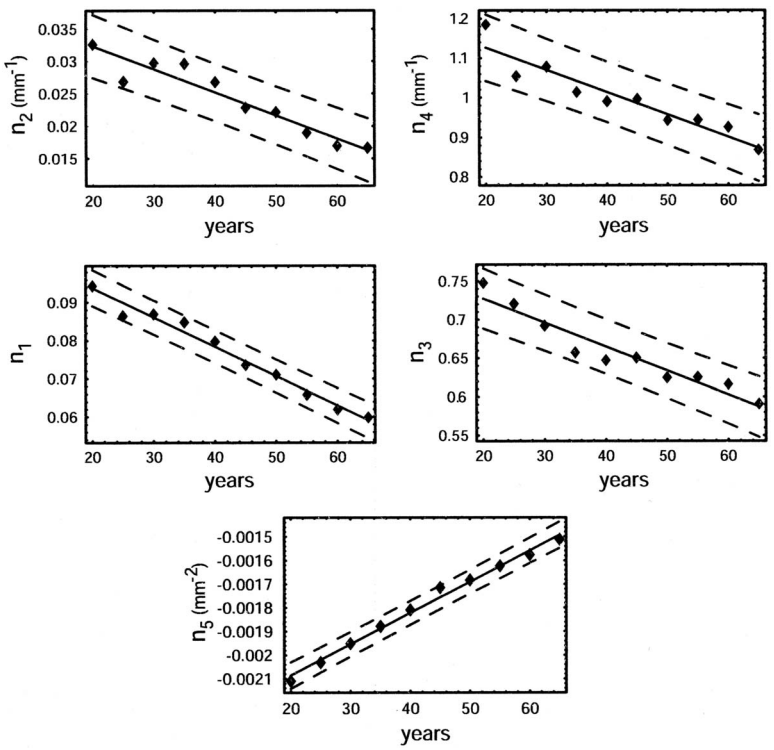

Fig. 3. GRIN profile parameters as a function of age (symbols). The solid line is the linear fit of the data, and the dashed lines represent the confidence interval at 95%.

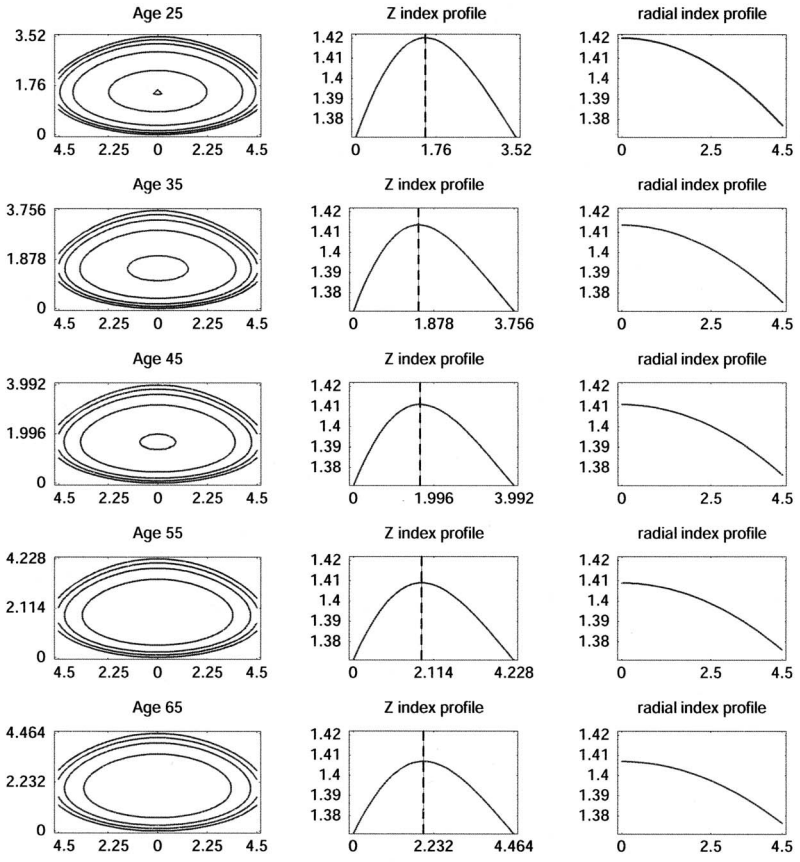

Fig. 4. Contour index values in the equatorial *YZ* plane (left column), index profile along the lens axis (middle column) and index variation of the lens-center index along the equatorial radius (right column) at different ages. The dashed line in the graphs corresponding to the index profile along the lens axis indicates the position of the lens-center-index value.

As reported in Table 1, the values obtained for the asphericities of the lens surfaces in a preliminary approach to GRIN profile modeling are −4.56 and −1.13. With these values, the ocular SA at 555 nm was evaluated by calculating the Zernike coefficient Z_4^0. The resulting value was 0.08 μm at 25 years for a 6 mm pupil diameter, this being less than that reported by Atchison [9,79]. This coefficient varied from 0.001 μm to 0.13 μm at that pupil diameter, which is in the low range of the normal population. Furthermore, as expected, we found an increase in this coefficient value with increasing age. Moreover, we calculated the evolution of the root-mean-square (RMS) wavefront aberration, calculated from the Zernike coefficients up to the sixth order, plus seventh-order SA [75] at that wavelength, but excluding piston, tilt, astigmatism, and defocus. We also found an increase in the RMS value, as expected, with increasing age (from 0.18 μm to 0.24 μm).

The results concerning the retinal-image quality are represented in Fig. 7. In this figure the average MTF, at 543 nm and for a 6 mm pupil, is plotted for three subjects at 25, 40, and 55 years of age. They are compared with the data reported by Guirao *et al.* [34] for the same age groups. These results are also similar to those of McLellan *et al.* [35] using a spatially resolved refractometer for a group of subjects from 23 to 65 years of age. The agreement is good beyond the 15 cpd, and the differences in this region are close to the standard deviation of the experimental data reported [34,42]. As seen, the retinal-image quality declines with advancing age, this effect being more significant at low spatial frequencies. In addition, although the differences are found at low spatial frequencies, we should bear in mind that the eye model

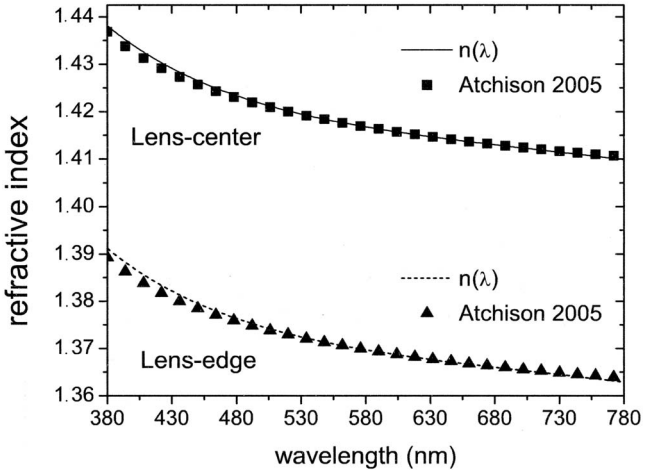

Fig. 5. Refractive index values corresponding to the lens edge and lens center (curves) as a function of wavelength compared to the data (symbols) from Atchison [9].

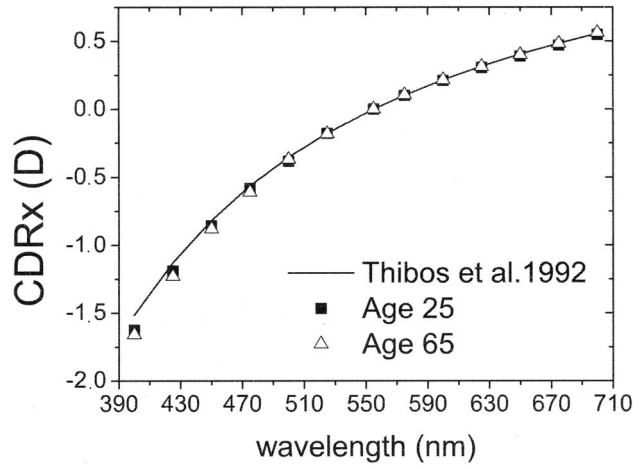

Fig. 6. Comparison of the chromatic difference on refraction (CDRx) corresponding to the ages of 25 and 65 years. Solid curve is that of the chromatic eye [57].

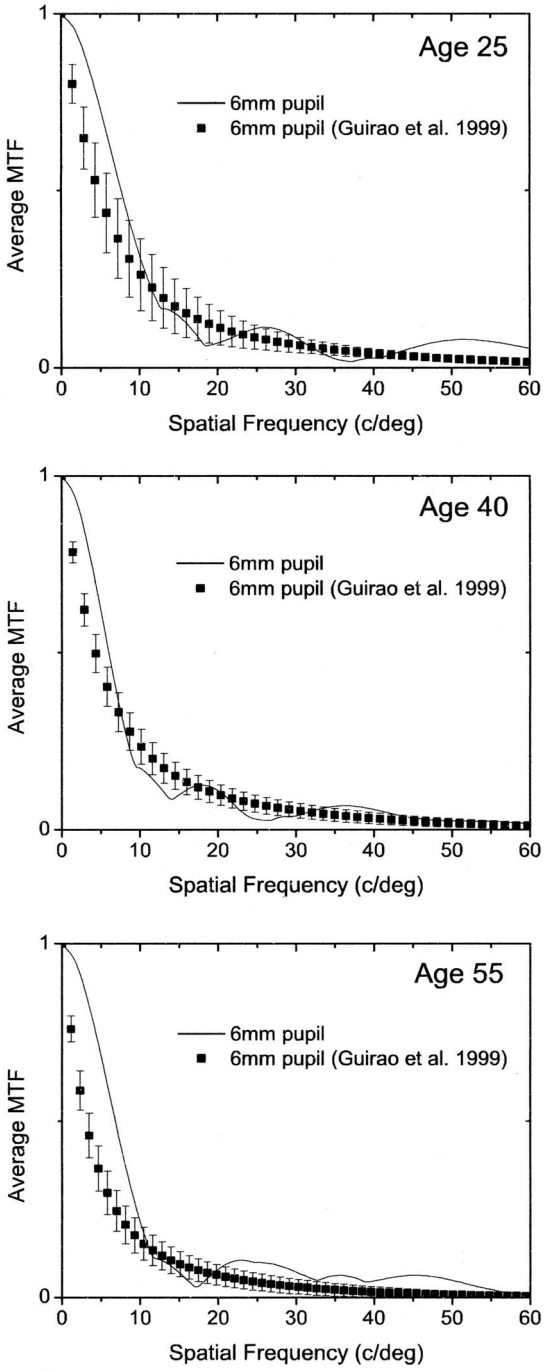

Fig. 7. Average modulation transfer function (MTF) at 543 nm for three representative ages, each one within the group adopted by Guirao *et al.* [34]. Data with the standard error from the normal population reported in that study are also plotted for comparison.

includes neither ocular scattering, nor corneal astigmatism, nor high-order aberrations, as we will discuss below.

4. DISCUSSION

We have modeled an anatomically accurate emmetropic age-dependent eye, taking into account recent ocular data regarding curvatures, asphericities, thicknesses, and media dispersions. In this schematic eye model, we need a lens having a single GRIN profile and dispersion properties as accurate as possible in order to account for the retinal-image-quality decrease with advancing age, for the increasing positive-wave SA, as well as for the constant longitudinal chromatic aberration. However, the model also has been constrained by the premise that the eye power should be constant with age and that the refractive index in the lens cortex should be 1.371, consistent with previous studies [19,21,54]. The model proposed also indicates a change in the asphericities of the lens surfaces in order to calculate the average value in the SA at 25 years. Though the value for the anterior lens surface asphericity is slightly modified ($Q_{l1}=-4.56$), that for the posterior one is substantially changed from $Q_{l2}=-4$ to $Q_{l2}=-1.13$, which is in the range of the normal population but closer to the values proposed by other schematic eye models [9,65,66]. Thus, the resulting value for the SA through the Zernike coefficient value, Z_4^0, is similar to the average value recently reported [9,79], and it increases with age. This shows the known effect regarding the change in the compensation of the SA, and even for high-order aberrations, between the cornea and the lens [80–85]. The lens geometry and GRIN profile change with age, decreasing the negative SA value. However, since the cornea does not change significantly, the overall SA of the eye becomes more positive with age, as the lens model in this study demonstrates.

The eye power was chosen as that determined for a 25-year-old subject, resulting in a value of 61.27 D. This value differs by 0.5 D, on average, with respect to previous models, and in some cases up to 1 D [7,22,64–66], but it agrees with the recent proposal [9] due mainly to the different eye axial length adopted, which was 23.59 mm compared with the widely accepted value of 24 mm. Once the eye power was kept constant with age, the results showed that a double modification in the GRIN profile must be performed to accomplish this. Thus, we can deduce from Fig. 4 that the lens-center-index value decreases and that its position along the lens axis also changes. This leads to the GRIN profile of the lens becoming more symmetrical along its axis as age increases.

Several works have attempted to explain why the eye power maintains its value with age, though the lens surfaces become steeper [19,49,50,53,54], i.e., the lens paradox. These works explain that a modification in the GRIN profile, as well as a change in the lens-center index could be responsible for it. Thus, Smith *et al.* [50] assume different theoretical parabolic and nonparabolic GRIN profiles for the lens-center-index variation along the equatorial radius, and they found that it would be necessary to change the parameters defining the different profiles to account for the constant eye power over age. Similar conclusions from experimental results were proposed by others [19,49,53,54]. Furthermore, some works [19,54] claim an additional needed variation in the lens-center-index value as small as 0.01, the same value found in the present study. However, recent results seem to indicate that the lens-center-index value does not change with age and that the size of the central index plateau increases in size also with age [21]. Then, the result would be an increase in the steepness of the index variation from the lens edge to the lens-center plateau with age.

Delving into the explanation of why the lens power remains constant over age, some works [21,50] have demonstrated that the GRIN lens power is the major contributor to the total lens power against the surface power. Therefore, there should be compensation between the GRIN power and the surface lens power—that is, a decrease in the GRIN power is needed since the surface power augments. Thus, for the age range considered, we have calculated the lens-surface power and the GRIN power from the *ABCD* formalism of the optical system in order to determine the first-order properties [86,87] (see Appendix A). This formalism, when applied to a lens having a GRIN profile described by isoindicial contours that are asymmetrical ellipses, gives a total power according to the expression [86]

$$\phi'_L = \phi'_G + \phi'_2 A_G + \phi'_1 D_G - \phi'_1 \phi'_2 B_G / n, \tag{10}$$

where $\phi'_G = -n_e C_G$ is the power corresponding to the GRIN profile; ϕ'_1 and ϕ'_2 are the front and back surface lens powers, respectively; A_G, B_G, C_G, and D_G are the elements of the GRIN profile *ABCD* matrix [87]; and $n_e = 1.371$ is the lens-edge-index value.

Table 3 lists according to age the matrix elements, the powers of the surfaces, the power of the GRIN profile, and the contribution to the power due to the lens surfaces ($\phi'_L - \phi'_G$) at 555 nm. As seen, it is demonstrated that the GRIN power is the main contributor to the lens power, and a decrease in this power is needed to compensate the increasing power by the contribution of the surfaces. In fact, if we assume that the GRIN profile does not change with age, i.e., the GRIN profile at 25 years is maintained over the age range, we find an increasing eye power with age, from 60.97 D to 63.66 D, causing progressive myopia; this supports previously published predictions of an increase in eye power of 2.5–3 D with age [50]. Moreover, there would be a dramatic worsening in the retinal-image quality with age for emmetropic subjects at low spatial frequencies due to defocus, which is not observed in the experimental data reported in the literature.

The analysis corresponding to the longitudinal eye chromatic aberration agrees quite well with those works demonstrating that it is independent of age. The parameters characterizing the dispersion of the GRIN profile proposed do not depend on aging. This confirms our assumption of not considering the parameters defining the GRIN distribution to be dependent on aging. Maybe a more complex index could include this dependence, but the present study proves that this is not necessary. Moreover, we have calculated the CDRx even if the GRIN profile does not change with aging. The results give the values of −1.63 D and −1.65 D for 20 and 65 years, respectively, at 400 nm and 0.55 D and 0.54 D at 700 nm,

Table 3. Values of the *ABCD* Matrix Elements (A_G, B_G, C_G, D_G) of the GRIN Lens Profile, Anterior Lens Power (ϕ_1'), Posterior Lens Power (ϕ_2'), Surface Power ($\phi_L' - \phi_G'$), GRIN Power (ϕ_G'), and Total Lens Power (ϕ_L') as Age Increases

Age	A_G	B_G(mm)	$C_G(D)$	D_G	ϕ_1' (D)	ϕ_2' (D)	$\phi_L' - \phi_G'$ (D)	ϕ_G' (D)	ϕ_L' (D)
20	0.99989	3.34731	−10.392	0.96532	3.03	5.96	8.83	14.25	23.08
25	1.00479	3.45945	−10.4017	0.959416	3.11	5.97	8.93	14.26	23.19
30	0.99876	3.57997	−10.274	0.964415	3.19	5.97	8.99	14.09	23.08
35	0.99799	3.69642	−10.209	0.96402	3.28	5.98	9.08	14.0	23.08
40	0.9977	3.81277	−10.1451	0.963243	3.37	5.99	9.17	13.91	23.08
45	0.9978	3.92976	−9.9049	0.962541	3.47	6.0	9.26	13.58	22.84
50	0.966867	4.04563	−10.09	0.958305	3.57	6.0	9.36	13.72	23.08
55	0.996512	4.16215	−9.9286	0.962031	3.68	6.01	9.46	13.61	23.07
60	0.995904	4.27847	−9.9102	0.961538	3.79	6.02	9.57	13.59	23.16
65	0.995524	4.39507	−9.7603	0.961406	3.92	6.03	9.69	13.38	23.07

respectively. Thus, if we compare these values with those of the chromatic eye (−1.51 D and 0.55 D, respectively), it appears that longitudinal eye chromatic aberration is not significantly altered by a change in the GRIN lens profile with age.

Finally, the MTF results reasonably predict the values reported in previous studies [34,35,42]. Differences are found mainly in the low spatial frequencies, as reflected in Fig. 7, with these becoming more noticeable at older ages. Nevertheless, they are closer to the variation in the normal population at medium and high spatial frequencies [34,35]. Our values are calculated as the average between vertical and horizontal MTFs, while data from Guirao *et al.* are the radial average taken from the actual two-dimensional MTF. A small variation should be expected if our results were calculated from a radial average, since we are using a decentered system having an asymmetrical two-dimensional MTF due to the presence of astigmatism and coma aberrations. In addition, we should bear in mind that the study of Guirao *et al.* reported results from a double-pass experimental method. As it is known, this method for determining the MTF includes ocular scattering [88,89], which could underestimate the values, especially at low spatial frequencies, and this would become more noticeable with age, as ocular scattering also increases [88–90]. In fact, our MTF results with age are closer to those reported by McLellan *et al.* [35], particularly at medium and high spatial frequencies.

In addition, we should also recall that we assume a rotationally symmetric cornea, and this is a simplification. Data reported by some authors [48,91] demonstrate that the cornea has different curvatures along perpendicular axes—that is, it shows astigmatism and possibly high-order aberrations. Furthermore, we have not considered a decentration for the lens, either. As discussed above, there are results that provide individual lens decentrations [60]. An element decentration in an optical system introduces an additional amount of aberration that is absent in the present study. All these considerations could contribute to an additional decline in the image quality at low spatial frequencies as age increases [81] and to an increase in the values concerning the RMS wavefront found in this study. The RMS variation found with age, though less than that reported in other experimental studies, is within the variation of the normal population. However, we think these model features would belong to a more customized eye model to resemble a particular individual's retinal-image quality.

5. CONCLUSION

In summary, this study proposes a single GRIN profile that makes it possible not only to work with a single component for the whole crystalline lens in current eye models but also to account for age-dependent vision defects as well as eye chromatic aberration. Furthermore, it provides an explanation for the lens paradox. This GRIN lens could be included in schematic eye models for performing visual simulations and for making predictions with respect to modern popular ophthalmic surgical procedures, modeling myopia, and accommodation effects on vision.

APPENDIX A: *ABCD* MATRIX OF THE CRYSTALLINE LENS

The first-order properties of an optical system are well described by the *ABCD* matrix of the system. The crystalline lens of the human eye is thick and composed of two aspherical surfaces plus a GRIN material. Given that the GRIN profile of the lens is an asymmetrical bielliptic type, Pérez *et al.* have derived the expressions that enable the calculation of the matrix elements of a slab lens having a GRIN profile of that type. That *ABCD* matrix is given by [87]

$$ABCD_G = \begin{bmatrix} A_G & B_G \\ C_G & D_G \end{bmatrix} = \begin{bmatrix} H_f(d) & H_a(d) \\ \dot{H}_f(d) & \dot{H}_a(d) \end{bmatrix}, \qquad \text{(A1)}$$

where $H_a(d)$ and $\dot{H}_a(d)$ are the height and the slope, respectively, of an axial ray and $H_f(d)$ and $\dot{H}_f(d)$ are those corresponding to the field ray, with d being the thickness of the slab GRIN lens. It then follows that $\phi_G' = -n_e \dot{H}_f(d)$, where n_e is the refractive index value at the lens edge.

Since the crystalline lens has two curved surfaces, we can apply the cascade matrix product to obtain the *ABCD* matrix of the whole crystalline. Thus, we can calculate [86]

$$ABCD_L = \begin{bmatrix} A_L & B_L \\ C_L & D_L \end{bmatrix} = R_2 ABCD_G R_1 = \begin{bmatrix} 1 & 0 \\ -\phi_2'/n_v & n_e/n_v \end{bmatrix} \times \begin{bmatrix} A_G & B_G \\ C_G & D_G \end{bmatrix} \begin{bmatrix} 1 & 0 \\ -\phi_1'/n_e & n_a/n_e \end{bmatrix}, \quad \text{(A2)}$$

in which R_1 and R_2 are the refraction matrices corresponding to the anterior and posterior crystalline surfaces, respectively; $ABCD_G$ is the GRIN profile matrix; and $n_a = n_v$ is the index value of the aqueous and vitreous humor, respectively, at 555 nm. Therefore, the power of the GRIN lens will be

$$\phi_L' = -C_L = \phi_G' + \phi_2' A_G + \phi_1' D_G - \phi_1' \phi_2' B_G / n_e, \quad \text{(A3)}$$

which is an equation equivalent to the power of a three-component system (see the Appendix in [86]).

ACKNOWLEDGMENTS

The authors are grateful for the financial support given by the CICYT (Ministerio de Ciencia y Tecnología, Spain) through grants BFM2003-1492 and DPI2005-08443-C02-02. The authors wish to thank D. A. Atchison (School of Optometry at the Queensland University of Technology) and G. Smith (Department of Optometry and Vision Sciences at the University of Melbourne) for their comments and suggestions in an earlier draft of this paper, and those from the reviewers for improving the scientific content and clarity of the manuscript. For ZEMAX users who are interested, the dynamic link library programmed (DLL library) for the GRIN profile used in this study is available from the corresponding author (J. A. Díaz).

REFERENCES

1. L. Matthiessen, "Untersuchungen über den aplanatismus und die periscopie der krystalllinsen in den augen der fische," Pfluegers Arch. Gesamte Physiol. Menschen Tiere **231**, 287–307 (1880).
2. L. Matthiessen, "Untersuchungen über den aplanatismus und die periscopie der krystalllinsen in den augen der fische," Pfluegers Arch. Gesamte Physiol. Menschen Tiere **27**, 510–523 (1882).
3. A. Gullstrand, *Hemholtz's Handbuch der Physiologischen Optik*, 3rd. ed., English translation edited by J. P. Southall (Optical Society of America, 1924), Vol. 1, Appendix II, pp. 301–358.
4. J. W. Blaker, "Toward an adaptative model of the human eye," J. Opt. Soc. Am. **70**, 220–283 (1980).
5. J. W. Blaker, "A comprehensive optical model of the aging, accommodating adult eye," in *Techical Digest on Ophthalmic and Visual Optics*, Vol. 2 of 1991 OSA Technical Digest Series (Optical Society of America, 1991), p. 2831.
6. D. A. Atchison and G. Smith, "Continuous gradient index and shell models of the human lens," Vision Res. **35**, 2529–2538 (1995).
7. H. Liou and N. A. Brennan, "Anatomically accurate, finite model eye for optical modeling," J. Opt. Soc. Am. A **14**, 1684–1695 (1997).
8. H. T. Kasprzak, "New approximation for the whole profile of the human crystalline lens," Ophthalmic Physiol. Opt. **20**, 31–43 (2000).
9. D. A. Atchison, "Optical models for human myopic eyes," Vision Res. **46**, 2236–2250 (2006).
10. B. K. Pierscionek, "Refractive index contours in the human lens," Exp. Eye Res. **64**, 887–893 (1997).
11. B. K. Pierscionek, "Surface refractive of the eye lens determined with an optical fiber sensor," J. Opt. Soc. Am. A **10**, 1867–1871 (1993).
12. B. K. Pierscionek, D. Y. C. Chan, J. P. Ennis, G. Smith, and R. C. Augusteyn, "Nondestructive method of constructing three dimensional gradient index models for crystalline lenses: 1. theory and experiment," Am. J. Optom. Physiol. Opt. **65**, 481–491 (1988).
13. B. K. Pierscionek, "Refractive index of the human lens surface measured with an optic fiber sensor," Ophthalmic Res. **26**, 32–35 (1994).
14. B. K. Pierscionek and D. Y. C. Chan, "Refractive index gradient of human lenses," Optom. Vision Sci. **66**, 822–829 (1989).
15. S. Nakao, S. Fujimoto, R. Nagata, and K. Iwata, "Model of the refractive-index distribution in the rabbit crystalline lens," J. Opt. Soc. Am. **58**, 1125–1130 (1968).
16. P. P. Fagerholm, B. T. Philipson, and B. Lindström, "Normal human lens, the distribution of protein," Exp. Eye Res. **33**, 615–620 (1981).
17. E. Acosta, R. Flores, D. Vazquez, S. Rios, L. F. Garner, and G. Smith, "Tomographic method for measurement of the refractive index profile of optical fibre forms and rod GRIN lenses," Jpn. J. Appl. Phys., Part 1 **41**, 4821–4824 (2002).
18. E. Acosta, D. Vazquez, R. Flores, L. F. Garner, and G. Smith, "Tomographic method for measurement of the gradient refractive index of the crystalline lens. I. The spherical fish lens," J. Opt. Soc. Am. A **22**, 424–433 (2005).
19. B. A. Moffat, D. A. Atchison, and J. M. Pope, "Age-related changes in the refractive index distribution and power of the human lens as measured by magnetic resonance micro-imaging *in vitro*," Vision Res. **42**, 1683–1693 (2002).
20. E. Acosta, D. Vazquez, R. Flores, L. F. Garner, and G. Smith, "Tomographic method for measurement of the gradient refractive index of the crystalline lens. II. The rotationally symmetrical lens," J. Opt. Soc. Am. A **23**, 2551–2565 (2006).
21. C. E. Jones, D. A. Atchison, R. Meder, and J. M. Pope, "Refractive index distribution and optical properties of the isolated human lens measured using magnetic resonance imaging (MRI)," Vision Res. **45**, 2352–2366 (2005).
22. O. Pomerantzeff, M. Pankratov, G. J. Wang, and P. Dufault, "Wide-angle optical mode of the eye," Am. J. Optom. Physiol. Opt. **61**, 166–176 (1984).
23. O. Pomerantzeff, P. Dufault, and R. Goldstein, "Wide-angle model of the eye," in *Advances in Diagnostic Visual Optics*, Springer Series in Optical Sciences, G. Breinin and I. Siegel, eds. (Springer-Verlag, 1983), pp. 12–21.
24. O. Pomerantzeff, H. Fish, J. Govingnon, and C. L. Schepens, "Wide-angle optical model of the human eye," Ann. Ophthalmol. **3**, 815–819 (1971).
25. E. H. Roth and G. Kluxen, "*In vivo* measurements of the distribution of the refractive index of the human lens with a Sheimpflug procedure of the anterior segment of the eye and a He–Ne laser beam," Fortschr. Ophthalmol. **87**, 312–316 (1990).
26. J. A. Díaz, R. G. Anera, J. R. Jiménez, and L. J. del Barco, "Optimum corneal asphericity of myopic eyes for refractive surgery," J. Mod. Opt. **50**, 1903–1915 (2003).
27. J. A. Díaz, J. A. Martínez, R. G. Anera, and J. R. Jiménez, "Permissible lateral misaligments in corneal ablation for myopic eyes," J. Opt. A, Pure Appl. Opt. **7**, 364–367 (2005).
28. D. A. Atchison and W. N. Charman, "Influence of reference plane and direction of measurement on eye aberration measurement," J. Opt. Soc. Am. A **22**, 2589–2597 (2005).
29. J. T. Holladay, P. A. Piers, G. Koranyi, M. van der Nooren, and N. E. S. Norby, "A new intraocular lens design to reduce spherical aberration of pseudophakic eyes," J. Refract. Surg. **18**, 683–691 (2002).
30. P. Piers, N. E. S. Norby, and U. Mester, "Eye models for the prediction of contrast vision in patients with new intraocular lens designs," Opt. Lett. **29**, 733–735 (2004).
31. J. A. Díaz, M. Irlbauer, and J. A. Martínez, "Diffractive–refractive hybrid doublet to achromatize the human eye," J. Mod. Opt. **51**, 2223–2234 (2004).

32. M. F. Deering, "A photon accurate model of the human eye," ACM Trans. Graphics **24**, 649–658 (2005).
33. Y. Benny, S. Manzanera, P. Prieto, E. Ribak, and P. Artal, "Wide-angle chromatic aberration corrector for the human eye," J. Opt. Soc. Am. A **24**, 1538–1544 (2007).
34. A. Guirao, C. González, M. Redondo, E. Geraghty, N. E. S. Norby, and P. Artal, "Average optical performance of the human eye as a function of age in a normal population," Invest. Ophthalmol. Visual Sci. **40**, 210–213 (1999).
35. J. S. McLellan, S. Marcos, and S. A. Burns, "Age-related changes in monochromatic wave aberrations of the human eye," Invest. Ophthalmol. Visual Sci. **42**, 1390–1395 (2001).
36. T. Fujikado, T. Kuroda, S. Nimomiya, N. Maeda, Y. Tanao, Y. Hirohara, and T. Mihashi, "Age-related changes of ocular and corneal aberrations," Am. J. Ophthalmol. **183**, 143–146 (2002).
37. D. A. Atchison, M. J. Collins, C. F. Wildsoet, J. Christiensen, and M. D. Waterworth, "Measurements of monochromatic ocular aberrations of human eyes as a fuction of accommodation by the Howland aberroscope technique," Vision Res. **35**, 313–323 (1995).
38. J. C. He, S. A. Burns, and S. Marcos, "Monochromatic aberrations in the accommodated human eye," Vision Res. **40**, 41–48 (2000).
39. H. Cheng, J. K. Barnett, A. S. Vilipuru, J. D. Marsack, S. Kasthuriragan, R. A. Applegate, and A. Roorda, "A population study on changes in wave aberrations with accommodation," J. Vision **16**, 272–280 (2004).
40. A. Popiolek-Masajada and H. Kasprzak, "Model of the optical system of the human eye during accommodation," Ophthalmic Physiol. Opt. **22**, 201–208 (2002).
41. Y. Huang and D. T. Moore, "Human eye modelling using a single equation of gradient index crystalline lens for relaxed and accommodated states," in *International Optical Design Conference*, G. G. Gregory, J. M. Howard, and R. J. Koshel, eds. (SPIE, 2006), Vol. 6342, pp. 6342D1–6342D9.
42. P. Artal, M. Ferro, I. Miranda, and R. Navarro, "Effects of aging in retinal image quality," J. Opt. Soc. Am. A **10**, 1656–1662 (1993).
43. R. I. Calver, M. J. Cox, and D. B. Elliot, "Effect of aging on the monochromatic aberrations of the human eye," J. Opt. Soc. Am. A **16**, 2069–2078 (1999).
44. G. Smith, M. Cox, R. Calver, and L. Garner, "The spherical aberration of the crystalline lens of the human eye," Vision Res. **41**, 235–243 (2001).
45. M. Dubbleman, G. L. van der Heijde, and H. A. Weeber, "The thickness of the aging human lens obtained from corrected Scheimpflug images," Optom. Vision Sci. **78**, 411–416 (2001).
46. M. Dubbleman, G. L. van der Heijde, and H. A. Weeber, "Change in the shape of the aging human crystalline lens with accommodation," Vision Res. **45**, 117–132 (2005).
47. M. Dubbleman, G. L. van der Heijde, H. A. Weeber, and G. Vrensen, "Change in the internal structure of the human crystalline lens with age and accommodation," Vision Res. **43**, 2363–2375 (2003).
48. M. Dubbleman, V. A. D. P. Sicam, and G. L. van der Heijde, "The shape of the anterior and posterior surface of the aging human cornea," Vision Res. **46**, 993–1001 (2006).
49. M. Dubbleman and G. L. van der Heijde, "The shape of the human lens: curvature, equivalent refractive index and the lens paradox," Vision Res. **41**, 1867–1877 (2001).
50. G. Smith, D. A. Atchison, and B. K. Pierscionek, "Modeling the power of the aging human eye," J. Opt. Soc. Am. A **9**, 2111–2117 (1992).
51. R. P. Hemenger, L. F. Garner, and S. C. Ooi, "Change with age of the refractive index gradient of the human ocular lens," Invest. Ophthalmol. Visual Sci. **36**, 703–707 (1995).
52. G. Smith, B. K. Pierscionek, and D. A. Atchison, "The optical modeling of the human lens," Ophthalmic Physiol. Opt. **11**, 359–369 (1991).
53. A. Glasser and M. C. W. Campbell, "Presbyopia and the optical changes in the human crystalline lens with age," Vision Res. **38**, 209–229 (1998).
54. B. A. Moffat, D. A. Atchsion, and J. M. Pope, "Explanation of the lens paradox," Optom. Vision Sci. **79**, 148–150 (2002).
55. D. A. Atchison and G. Smith, "Chromatic dispersion of the ocular media of human eyes," J. Opt. Soc. Am. A **22**, 29–37 (2005).
56. R. E. Bedford and G. Wyszecki, "Axial chromatic aberration of the human eye," J. Opt. Soc. Am. **37**, 564–565 (1947).
57. L. N. Thibos, M. Ye, X. Zhang, and A. Bradley, "The chromatic eye: a new reduced-eye model of ocular chromatic aberration in humans," Appl. Opt. **31**, 3594–3600 (1992).
58. A. Morrell, H. D. Whitefoot, and W. N. Charman, "Ocular chromatic aberration and age," Ophthalmic Physiol. Opt. **11**, 385–390 (1991).
59. P. A. Howarth, X. Zhang, A. Bradley, D. L. Still, and L. N. Thibos, "Does the chromatic aberration of the eye vary with age?" J. Opt. Soc. Am. A **5**, 2087–2092 (1988).
60. Y. Chang, H.-M. Wu, and Y.-F. Lin, "The axial misalignment between ocular lens and cornea observed by MRI(I)—at fixed accommodative state," Vision Res. **47**, 71–84 (2007).
61. J. Tabernero, A. Benito, V. Nourrit, and P. Artal, "Instrument for measuring the misalignment of ocular surfaces," Opt. Express **14**, 10945–10956 (2006).
62. D. A. Atchison, N. Pritchard, K. L. Schmid, D. H. Scott, C. Jones, and J. Pope, "Shape of the retinal surface in emmetropia and myopia," Invest. Ophthalmol. Visual Sci. **46**, 2698–2707 (2005).
63. D. Atchison and G. Smith, *Optics of the Human Eye* (Butterwoth-Heinemann, 2000).
64. A. C. Kooijman, "Light distribution on the retina of a wide-angle theoretical eye," J. Opt. Soc. Am. **73**, 1544–1550 (1983).
65. R. Navarro, J. Santamaría, and J. Bescós, "Accommodation-dependent model of the human eye with aspherics," J. Opt. Soc. Am. A **2**, 1273–1281 (1985).
66. I. Escudero-Sanz and R. Navarro, "Off-axis aberrations of a wide-angle schematic eye," J. Opt. Soc. Am. A **16**, 1881–1891 (1999).
67. Y. Yang, K. Thompson, and S. A. Burns, "Pupil location under mesopic, phottopic, and pharmacologically dilated conditions," Invest. Ophthalmol. Visual Sci. **43**, 2508–2512 (2002).
68. P. Rosales, M. Dubbleman, S. Marcos, and G. van der Heijde, "Crystalline lens radii of curvature from Purkinje and Scheimpflug imaging," J. Vision **6**, 1057–1067 (2006).
69. W. J. Tropf, M. E. Thomas, and T. J. Harris, "Optical properties of crystal and glasses," in *Handbook of Optics* (Optical Society of America, 1995), Vol. 2, pp. 33.25–33.28.
70. J. P. Carroll, "Apodization model of the Stiles–Crawford effect," J. Opt. Soc. Am. **70**, 1155–1156 (1980).
71. D. A. Atchison, A. Joblin, and G. Smith, "Influence of Stiles–Crawford effect apodization on spatial visual performance," J. Opt. Soc. Am. A **15**, 2545–2551 (1998).
72. D. A. Atchison, D. H. Scott, A. Joblin, and G. Smith, "Influence of Stiles–Crawford effect apodization on spatial visual performance with decentered pupils," J. Opt. Soc. Am. A **18**, 1201–1211 (2001).
73. S. A. Burns and S. Marcos, "Measurement of the image quality of the eye with a spatially resolved refractometer," in *Customized Corneal Ablations* (Slack, 2001), pp. 201–209.
74. G. Wyszecki and W. S. Stiles, *Color Science: Formula and Quantitative Data* (Wiley, 1982).
75. L. N. Thibos, R. A. Applegate, J. T. Schwiegerling, R. Webb, and V. S. T. Members, "Standards for reporting the optical aberrations of eyes," Opt. Photonics News **35**, 232–244 (2000).
76. R. R. Shannon, *The Art and Science of Optical Design* (Cambridge U. Press, 1997).
77. R. E. Fisher and B. Tadic-Galeb, *Optical System Design* (McGraw-Hill, 2000).
78. ZEMAX Development Corporation, *ZEMAX Optical Design Program: User's Guide, Version 10* (Zemax Software Development, 2004).
79. D. A. Atchison, "Recent advances in measurement of monochromatic aberrations of human eyes," Clin. Exp. Optom. **88**, 5–27 (2005).

80. P. Artal and A. Guirao, "Contribution of cornea and lens to the aberrations of the human eye," Opt. Lett. **23**, 1713–1715 (1998).
81. P. Artal, E. Berrio, and A. Guirao, "Contribution of the cornea and internal surfaces to the change of ocular aberrations with age," J. Opt. Soc. Am. A **19**, 137–143 (2002).
82. P. Artal, A. Guirao, E. Berrio, and D. Williams, "Compensation of corneal aberrations by the internal optics in the human eye," J. Vision **1**, 1–8 (2001).
83. J. Kelly, T. Mihashi, and H. Howland, "Compensation of corneal horizontal/vertical astigmatism, lateral coma and spherical aberration by internal optics of the eye," J. Vision **4**, 262–271 (2004).
84. P. Artal, A. Benito, and J. Tabernero, "The human eye is an example of robust optical design," J. Vision **4**, 1–7 (2006).
85. J. Tabernero, A. Benito, E. Alarcón, and P. Artal, "Mechanism of compensation of aberrations in the human eye," J. Opt. Soc. Am. A **24**, 3274–3283 (2007).
86. M. V. Pérez, C. Bao, M. T. Flores-Arias, M. A. Rama, and C. Gómez-Reino, "Description of gradient-index crystalline lens by a first order optical system," J. Opt. A, Pure Appl. Opt. **7**, 103–110 (2005).
87. M. V. Pérez, C. Bao, M. T. Flores-Arias, M. Rama, and C. Gómez-Reino, "Gradient parameter and axial and field rays in the gradient-index crystalline lens model," J. Opt. A, Pure Appl. Opt. **5**, S293–S297 (2003).
88. F. Díaz-Douton, A. Benito, J. Pujol, M. Arjona, J. Guillen, and P. Artal, "Comparison of the retinal image quality with a Hartmann comparison of the retinal image quality with a Hartmann–Shack wavefront sensor and a double-pass instrument," Invest. Ophthalmol. Visual Sci. **47**, 1710–1716 (2006).
89. P. Rodríguez and R. Navarro, "Double-pass versus aberrometric modulation transfer function in green light," J. Biomed. Opt. **12**, 0440181 (2007).
90. R. P. Hemenger, "Intraocular light scattering in normal vision loss with age," Appl. Opt. **23**, 1972–1974 (1984).
91. M. C. Dunne, J. M. Royston, and D. A. Barnes, "Posterior corneal surface toricity and total corneal astigmatism," Optom. Vision Sci. **68**, 708–710 (1991).